PTP1B inhibition suggests a therapeutic strategy for Rett syndrome

Navasona Krishnan,[1] Keerthi Krishnan,[1] Christopher R. Connors,[2] Meng S. Choy,[2] Rebecca Page,[3] Wolfgang Peti,[2] Linda Van Aelst,[1] Stephen D. Shea,[1] and Nicholas K. Tonks[1]

[1]Cold Spring Harbor Laboratory (CSHL), Cold Spring Harbor, New York, USA. [2]Department of Molecular Pharmacology, Physiology and Biotechnology, and [3]Department of Molecular Biology, Cell Biology and Biochemistry, Brown University, Providence, Rhode Island, USA.

The X-linked neurological disorder Rett syndrome (RTT) presents with autistic features and is caused primarily by mutations in a transcriptional regulator, methyl CpG–binding protein 2 (MECP2). Current treatment options for RTT are limited to alleviating some neurological symptoms; hence, more effective therapeutic strategies are needed. We identified the protein tyrosine phosphatase PTP1B as a therapeutic candidate for treatment of RTT. We demonstrated that the *PTPN1* gene, which encodes PTP1B, was a target of MECP2 and that disruption of MECP2 function was associated with increased levels of PTP1B in RTT models. Pharmacological inhibition of PTP1B ameliorated the effects of MECP2 disruption in mouse models of RTT, including improved survival in young male (*Mecp2*$^{-/y}$) mice and improved behavior in female heterozygous (*Mecp2*$^{-/+}$) mice. We demonstrated that PTP1B was a negative regulator of tyrosine phosphorylation of the tyrosine kinase TRKB, the receptor for brain-derived neurotrophic factor (BDNF). Therefore, the elevated PTP1B that accompanies disruption of MECP2 function in RTT represents a barrier to BDNF signaling. Inhibition of PTP1B led to increased tyrosine phosphorylation of TRKB in the brain, which would augment BDNF signaling. This study presents PTP1B as a mechanism-based therapeutic target for RTT, validating a unique strategy for treating the disease by modifying signal transduction pathways with small-molecule drugs.

Introduction

Rett syndrome (RTT) is a neurological disorder that affects approximately 1 in 10,000 female births (1), an incidence similar to that of cystic fibrosis and Huntington's disease. Girls with RTT develop normally during the first 6 months of life but then begin to present a host of neurodevelopmental abnormalities including learning disabilities, loss of motor skills, stereotypic hand movements, irregular breathing, and seizures (1, 2). Boys are more severely affected and tend not to survive infancy due to encephalopathy (3). Patients with RTT also exhibit deficits in social interactions, a feature reminiscent of autism.

In over 95% of cases, RTT is caused by mutations in the X-linked methyl CpG–binding protein 2 (*MECP2*) gene, which was the first autism spectrum disorder gene to be identified (4). MECP2 is an epigenetic factor that binds to methylated DNA to regulate chromatin structure and the expression of a wide range of genes throughout the genome (5, 6). Although there are recognizable methyl CpG–binding and transcription repression domains, MECP2 is predominantly an intrinsically disordered protein that participates in a variety of protein-protein interactions and is subject to various posttranslational modifications, all of which contribute to its functional diversity (6). Hundreds of pathogenic *MECP2* mutations have been identified, approximately half of which are associated with the methyl CpG–binding domain, focusing attention on its function as a regulator of gene expression (6). Mice lacking an intact *Mecp2* gene have been shown to recapitulate a broad spectrum of phenotypes with similarities to those encountered in RTT patients (7–9). As in human patients, deficits are more pronounced in males than in females, with hemizygous null males being more severely affected by encephalopathy (7). In the heterozygous female (*Mecp2*$^{-/+}$) mice, random X chromosome inactivation results in mosaic expression of MECP2 in the brain, with some cells expressing the mutant and others the normal allele, which likely contributes to phenotypic variations.

At present, these broad effects of MECP2 represent a challenge for drug development, and there is no disease-modifying therapy for RTT; instead, the focus has been on managing symptoms (1, 10). RTT has been associated with structural changes in the brain including reduced size and weight, together with effects on neuronal density and cell morphology (1, 2). Such abnormalities have often been viewed as irreversible; however, there have been studies to show that after disease onset in mice lacking the gene, restoration of MECP2 expression can rescue most neurological deficits and improve survival (7). This indicates that symptoms associated with *Mecp2* loss can be reversed, focusing attention on reversible effects on neural circuits rather than on irreversible effects on development. There has been discussion in the field of future gene therapy approaches based on restoration of MECP2 function; however, considering the broad effects of MECP2 on the regulation of chromatin structure and gene expression and the important role of MECP2 in postmitotic neurons, it is unlikely that such approaches will provide an immediate solution. Instead, the field has begun to consider signaling events that may be subject to the influence of MECP2.

▶ Related Commentary: p. 2931

Conflict of interest: The authors have declared that no conflict of interest exists.
Submitted: December 4, 2014; **Accepted:** June 5, 2015.
Reference information: *J Clin Invest*. 2015;125(8):3163–3177. doi:10.1172/JCI80323.

The neurotrophic factor brain-derived neurotrophic factor (BDNF) was identified as a target of MECP2, the levels of which are decreased in RTT. Experimental approaches to elevate BDNF ameliorated some symptoms (11), and alternative approaches using BDNF mimetics are being tested (12); however, the therapeutic utility of these mimetics remains to be established. Levels of insulin-like growth factor 1 (IGF-1) are also reduced in *Mecp2*-mutant mice (13), and treatment with an N-terminal tripeptide derived from IGF-1 has been reported to ameliorate some symptoms of RTT in these animals (13). In fact, these agents have formed the basis of clinical trials for this indication (13). In an alternative approach involving mutagenesis screens in *Mecp2*-mutant mice, mutations in squalene epoxidase, the rate-limiting enzyme in cholesterol biosynthesis, were identified as suppressing RTT-associated phenotypes. Interestingly, cholesterol metabolism is altered and cholesterol levels are elevated in the brains of *Mecp2*$^{-/y}$ male mice, all of which prompted the testing of statins with positive effects on some, but not all, categories of symptoms (14). Loss of function of MECP2 has also been associated with disruption of signaling through the AKT/mTOR pathway (15). Activation of this classical signaling pathway by adding exogenous growth factors or by suppressing the tumor suppressor PTEN ameliorated the effects of loss of MECP2 in neuronal cell models, suggesting that there may be beneficial effects of manipulating cell signaling to promote protein synthesis (15).

Instead of considering RTT in terms of alterations of specific driver genes, we looked at common phenotypic features that may suggest therapeutic targets. We noted that obesity and leptin resistance have been reported in some mouse models (16). In addition, insulin resistance has also been noted in some RTT patients (17). Furthermore, obesity is becoming recognized as a common feature of autism spectrum disorders (18). We further investigated this aspect of metabolic disruption in RTT and demonstrated that glucose metabolism and insulin signaling in the brain were attenuated in *Mecp2*-mutant mice. This suggested to us the possibility of a role for the protein tyrosine phosphatase PTP1B, which is recognized as a major metabolic regulator that is known to attenuate both insulin and leptin signaling (19). PTP1B inhibits insulin signaling by dephosphorylating the β subunit of the insulin receptor (IR-β) and insulin receptor substrate 1 (IRS1), and attenuates leptin signaling by acting on the leptin receptor–associated tyrosine kinase JAK2 (19). Hence, it negatively regulates the downstream PI3K/AKT signaling pathway that is important for development and known to be attenuated in RTT models (15, 20).

In this study, we have demonstrated that the *PTPN1* gene, which encodes PTP1B, was a direct target of MECP2 and that PTP1B protein levels were dramatically increased in *Mecp2*-mutant mice and in fibroblasts derived from patients with RTT. We show that administration of small-molecule inhibitors of PTP1B to *Mecp2*-mutant mice restored glucose homeostasis and enhanced insulin-induced tyrosine phosphorylation and signaling in the brain. Treatment with PTP1B inhibitors dramatically extended the lifespan of *Mecp2*$^{-/y}$ male mice and improved the performance of *Mecp2*$^{-/+}$ female mice in behavioral assays. Finally, we demonstrated that PTP1B recognized TRKB as a direct substrate and that inhibition of PTP1B resulted in enhanced TRKB phosphorylation in the brains of *Mecp2*-mutant mice. Overall, through this study, we have validated PTP1B as a target for therapeutic intervention in RTT, offering a new strategy for treating this disease by modifying signal transduction pathways with small-molecule drugs.

Results

Insulin signaling and glucose metabolism were impaired in Mecp2-mutant mice. Metabolic dysregulation is associated with a number of neurodevelopmental disorders including RTT syndrome. Interestingly, it was previously noted that *Mecp2*$^{-/y}$ mice on a 129S6B6F1 background display an obese phenotype characterized by insulin resistance and increased serum levels of cholesterol and triglycerides (21); however, it is not clear whether disruption of *Mecp2* gene function results in impaired insulin signaling. We performed glucose and insulin tolerance tests (GTT and ITT) in both male *Mecp2*$^{-/y}$ (P30) and female *Mecp2*$^{-/+}$ (P70) mice to examine whether insulin signaling was altered in mouse models of RTT. Both hemizygous male *Mecp2*$^{-/y}$ and heterozygous female *Mecp2*$^{-/+}$ mice exhibited glucose intolerance and cleared glucose at a slower rate than did the control WT mice (Figure 1A). Furthermore, unlike the WT mice, blood glucose levels in both *Mecp2*$^{-/y}$ and *Mecp2*$^{-/+}$ mice failed to respond normally to administration of insulin (Figure 1B). We also found that insulin and cholesterol levels were higher in both *Mecp2*$^{-/y}$ and *Mecp2*$^{-/+}$ mice compared with levels in their WT counterparts (Supplemental Figure 1; supplemental material available online with this article; doi:10.1172/JCI80323DS1). Although glucose and insulin intolerance was observed in both male *Mecp2*$^{-/y}$ and female *Mecp2*$^{-/+}$ mice, it was more pronounced in male *Mecp2*$^{-/y}$ mice, which may reflect the difference in MECP2 expression levels.

To characterize this observation further, we examined the insulin-signaling response in both *Mecp2*$^{-/y}$ and *Mecp2*$^{-/+}$ mice. In the male *Mecp2*$^{-/y}$ mice, which are MECP2-null, insulin-induced tyrosine phosphorylation of IR-β and RS1 was markedly attenuated compared with the response observed in WT animals (Figure 1C). Recruitment of phosphorylated IRS1 to a complex with the insulin receptor (IR) triggers activation of phosphatidylinositol 3-kinase (PI3K) and stimulation of downstream signaling molecules such as PKB/AKT, which results in the inactivation of glycogen synthase kinase-3 β (GSK3β), the translocation of glucose transporters, and glucose uptake (22). Therefore, we examined phosphorylation of the kinase AKT and additional downstream signaling components. In contrast to the WT mice, *Mecp2*$^{-/y}$ mice displayed diminished insulin-induced phosphorylation of AKT and its substrates FOXO and GSK3β. Although the signaling response to insulin was diminished in the MECP2-mutant mice, these animals had higher circulating levels of the hormone (Supplemental Figure 1A). These are features of a classical example of insulin resistance. Similar trends of reduced tyrosine phosphorylation of IR-β and IRS1, together with decreased activation of AKT, were observed in female *Mecp2*$^{-/+}$ mice (Figure 1D). Consequently, the data suggest that these RTT models may also feature a metabolic disorder characterized by impaired insulin signaling and aberrant glucose metabolism. One poten-

tial mechanism for this effect would be that loss of expression of *Mecp2* resulted in an increase in the levels or activity of a protein tyrosine phosphatase that normally functions as an antagonist of insulin signaling. Therefore, we tested for the effects of *Mecp2* loss on gene expression in the mouse forebrain to identify candidates that are implicated in the control of insulin signaling (Figure 2A) and glucose metabolism (Supplemental Figure 2A) and regulated by MECP2.

Mecp2-mutant mice expressed elevated levels of PTP1B. Total RNA was isolated from the forebrains of *Mecp2*$^{-/y}$ (null) mice and their WT littermates. Our analysis by quantitative PCR (qPCR) revealed 4 genes that were upregulated by greater than 1.5-fold and 5 genes that were downregulated in the insulin-signaling pathway in *Mecp2*$^{-/y}$ mice compared with WT mice (Figure 2A). Since we were interested in identifying potential therapeutic targets, we focused our attention on genes that were upregulated in the *Mecp2*$^{-/y}$ animals. One of the 4 genes that was upregulated was *Ptpn1*, which encodes PTP1B, a protein tyrosine phosphatase that has been validated as a negative regulator of signaling in response to insulin and leptin (19); consequently, we tested whether *PTPN1* was a direct target of MECP2.

We used a series of reporter plasmids in which the expression of luciferase is driven by elements of the *PTPN1* promoter (23, 24). Upon coexpression of the reporter plasmids containing different lengths of the *PTPN1* promoter sequence, together with either isoform of MECP2 (MECP2-E1 and MECP2-E2), we observed that both isoforms of MECP2 suppressed *PTPN1* promoter activity (Figure 2B). Furthermore, unlike WT MECP2, expression of MECP2-R168X, a clinically relevant loss-of-function mutant, did not suppress *PTPN1* promoter activity (Figure 2C and Supplemental Figure 2C). These data suggest that *PTPN1* was a direct target of MECP2.

To confirm that MECP2 interacted with the *PTPN1* promoter, we carried out ChIP and examined several genes encoding known regulators of insulin signaling. Of those genes tested by ChIP analysis, we observed that MECP2 bound to the *PTPN1* promoter (Supplemental Figure 2B). Finally, to determine whether the increase in *Ptpn1* mRNA detected by qPCR correlated with the level of PTP1B protein in *Mecp2*-mutant mice, we subjected equal quantities of lysate from WT and *Mecp2*$^{-/y}$ brain sections to immunoblotting. We observed that in male mice lacking MECP2, expression of PTP1B protein was markedly elevated compared with the levels detected in their WT counterparts (Figure 2D). Similarly, expression of PTP1B was also higher in female *Mecp2*$^{-/+}$ mice (Figure 2E). Finally, consistent with our observation in MECP2-mutant mice, we observed elevated PTP1B protein levels in fibroblasts derived from patients with RTT (Figure 2F). These data illustrate that the *PTPN1* gene, encoding PTP1B, was a target of MECP2.

CPT157633 and UA0713 selectively inhibited PTP1B by 2 distinct mechanisms. In order to determine the significance of the elevated PTP1B levels in animal models of RTT, we tested the effects of small-molecule inhibitors of the phosphatase. Using para-nitro phenyl phosphate (pNPP) as a substrate, we studied PTP1B inhibition by CPT157633 (Figure 3A and ref. 25). The compound was found to be a high-affinity, competitive inhibitor of the phosphatase (Figure 3B), with an inhibition constant (K_I) of 40 nM. A similar result was obtained using ^{32}P-labeled RCML as a protein substrate (Figure 3C). Furthermore, we demonstrated that, compared with PTP1B, CPT157633 was markedly less effective against a panel of 6 PTPs and 2 dual-specificity phosphatases (Figure 3D), illustrating specificity in the effects of the inhibitor. To obtain structural insights into PTP1B-CPT157633 interaction, we used both biomolecular NMR spectroscopy and x-ray crystallography. Residues 1–301 from the catalytic domain of PTP1B were expressed in D_2O-based medium, and 2D [^{1}H,^{15}N] TROSY spectra were recorded in the absence and presence of CPT157633. NMR chemical shift perturbation (CSP) mapping showed that residues surrounding the active site were most affected by CPT157633 binding to the protein (Figure 3, E and F). This was confirmed by the crystal structure of the PTP-1B:CTP157633 complex (Supplemental Table 2 and Supplemental Figure 3), which illustrated a noncovalent interaction. Electrostatic interactions made by the compound to critical active site residues are highlighted in Figure 3G. Together, these data demonstrate that CPT157633 was a selective, reversible, active site–directed inhibitor of PTP1B.

To strengthen the functional analysis and ameliorate concerns about off-target effects of CPT157633, we characterized a second inhibitor of PTP1B that would exert its effect on the enzyme by a different mechanism. In our search for potent and selective inhibitors of the enzyme, we identified compounds with a triterpene structure, several of which were found to be noncompetitive inhibitors of PTP1B (26). Of those compounds assayed, UA0713 was found to be the most potent inhibitor of PTP1B (Supplemental Figure 4A and ref. 27). We observed that UA0713 was a noncompetitive inhibitor of PTP1B that inhibited the enzyme with a K_I of 150 nM (Supplemental Figure 4, B and C). It inhibited PTP1B with selectivity compared with a panel of 8 phosphatases investigated (Supplemental Figure 4D). Taken together, we have 2 high-affinity inhibitors of PTP1B that are structurally distinct and inhibit the enzyme by 2 distinct mechanisms.

Inhibition of PTP1B improved survival in Mecp2$^{-/y}$ *mice.* To investigate the extent to which the enhanced levels of PTP1B that were associated with MECP2 disruption could contribute to the RTT phenotype, we tested the effects of these 2 structurally and mechanistically distinct inhibitors of the phosphatase on WT and *Mecp2*$^{-/y}$-mutant mice. Two weeks after initiating treatment, we tested serum glucose levels and observed that the glucose intolerance encountered in untreated animals was markedly reduced (Figure 4A). In addition, we noted a small increase in BW in *Mecp2*$^{-/y}$ mice that were administered CPT157633 compared with that seen in saline-treated mice (Figure 4B), together with a decrease in circulating levels of insulin and cholesterol (Supplemental Figure 5, A and B). These data suggest that PTP1B inhibition resulted in an overall improvement in metabolism. Most strikingly, we observed that treatment with PTP1B inhibitors led to an approximately 2-fold increase in survival of the *Mecp2*$^{-/y}$-mutant mice (Figure 4C). The median lifespan was increased to 75 days following CPT157633 treatment and to 95 days for UA0713-treated mice, compared with 40 days for saline-treated animals.

As expected, treatment with the PTP1B inhibitors resulted in enhanced tyrosine phosphorylation of both IR-β and IRS1, 2

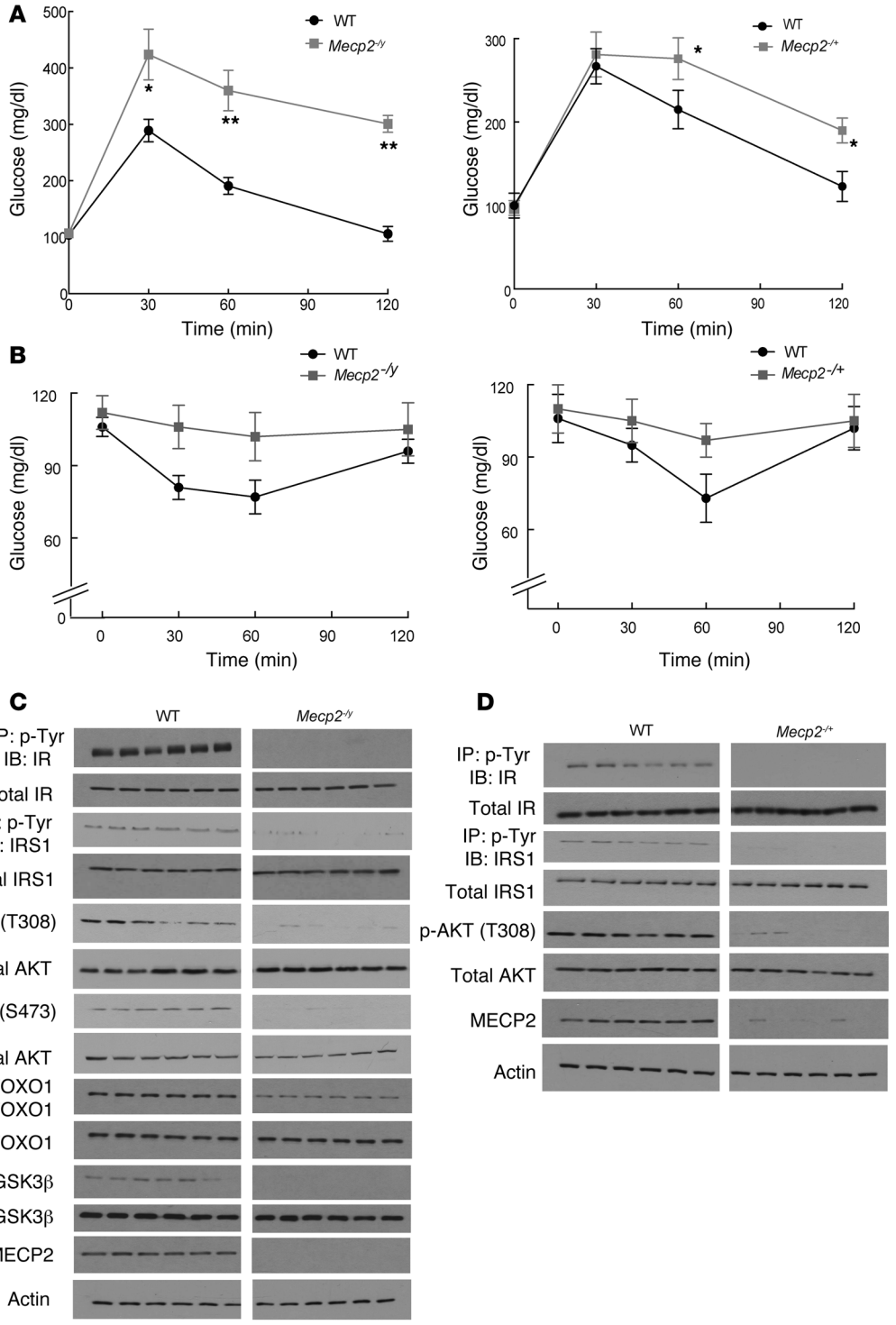

known substrates of the phosphatase (28, 29), compared with that observed in saline-treated controls (Figure 4D). In order to assess the significance of the ability of these inhibitors to restore glucose homeostasis, we tested 3 other small-molecule agents that have been shown to display antidiabetic properties, in particular metformin, rosiglitazone, and AICAR (30, 31). Interestingly, although treatment with each of these agents resulted in an improvement in glucose homeostasis (Supplemental Figure 5, C–E), none were as effective as the PTP1B inhibitors in extending the lifespan of the *Mecp2*$^{-/y}$-mutant mice (Figure 4E). Together, these data suggest that, as well as modifying insulin signaling and glucose homeostasis, inhibition of PTP1B may also alter additional signaling events that play a critical role in the RTT phenotype.

Inhibition of PTP1B ameliorated symptoms of RTT in Mecp2$^{-/+}$ *mice*. As heterozygous female *Mecp2*$^{-/+}$ mice are a closer reflection of RTT in humans than are male *Mecp2*-null mice, we also tested the inhibitors of PTP1B in these animals (32). As a first step, we tested the effects of CPT157633 administration on glu-

Figure 1. *Mecp2*-mutant mouse model displayed impaired insulin signaling and glucose metabolism. (**A**) GTT results for WT and *Mecp2*-mutant mice: 4-week-old male WT (n = 10) (black) or *Mecp2*$^{-/y}$ (n = 10) (gray) mice were administered D-glucose (2 mg/g BW), and blood glucose was monitored (left panel). GTT results for 8-week-old female WT (n = 10) (black) and *Mecp2*$^{-/+}$ (n = 10) (gray) mice are shown on the right. Statistical analysis was performed using 2-way ANOVA (**P < 0.01, *P < 0.05). (**B**) ITT results for WT and *Mecp2*-mutant mice: WT (n = 10; black) or *Mecp2*$^{-/y}$ (n = 10; gray) mice were administered insulin (0.75 mU/g BW), and blood glucose was monitored (left panel). ITT results for 8-week-old female *Mecp2*$^{-/+}$ (n = 10; gray) and WT (n = 10; black) mice are shown on the right. Statistical analysis was performed using 2-way ANOVA (P = 0.1). (**C**) Representative immunoblots for insulin signaling in WT and *Mecp2*$^{-/y}$ forebrain tissue lysates. Immunoblots showing insulin-induced tyrosine phosphorylation of IR-β and IRS1, threonine (T308) and serine (S473) phosphorylation of AKT, phosphorylation of FOXO1 and GSK3β, and their total protein levels in forebrain tissue lysates from 4-week-old WT and *Mecp2*$^{-/y}$ mice. For insulin stimulation, animals were treated with insulin (0.75 mU/g, i.p.) for 15 minutes. All blots are representative of experiments performed 3 times. (**D**) Representative immunoblots for insulin signaling in WT and *Mecp2*$^{-/+}$ forebrain tissue lysates. Immunoblots show insulin-induced tyrosine phosphorylation of IR-β and IRS1, T308 phosphorylation of AKT, and their total protein levels in forebrain tissue lysates from 8-week-old WT and *Mecp2*$^{-/+}$ mice. For insulin stimulation, animals were treated with insulin (0.75 mU/g, i.p.) for 15 minutes. All blots are representative of experiments performed 3 times.

cose homeostasis. Consistent with the observation in male mice, we observed that the glucose intolerance encountered in saline-treated female *Mecp2*$^{-/+}$ mice was ameliorated within 3 weeks of treatment with the inhibitor (Figure 5A). Consistently, we also saw an improvement in insulin signaling (Figure 5B). Therefore, we tested whether treatment with CPT157633 also had an impact on neural and behavioral symptoms in *Mecp2*$^{-/+}$ mice.

Paw clasping is a classic phenotype consistently observed in *Mecp2*$^{-/+}$ mice, and it is similar to the characteristic hand wringing that is commonly noted in patients with RTT (33). When lifted by the tail, WT mice extended their limbs, whereas, in contrast, *Mecp2*$^{-/+}$ mice clasped their front paws spontaneously for the entire length of time they were monitored, without any significant movement of the paws. Interestingly, *Mecp2*$^{-/+}$ mice that were administered CPT157633, showed a marked reduction in paw clasping, and extended their paws in a manner similar to that of WT animals (Figure 5C).

Regression of motor skills is also one of the common symptoms associated with RTT in patients and is also observed in *Mecp2*$^{-/+}$ mice. To test whether inhibition of PTP1B resulted in improved motor skills, we subjected saline- and CPT157633-treated WT and *Mecp2*$^{-/+}$ mice to a rotarod performance test. In comparison with WT mice, the *Mecp2*$^{-/+}$ mice showed lower levels of activity on the rotarod. In 4 successive trials of the WT mice, a dramatic improvement was observed in the time spent on the rotating rod, whereas no improvement was observed with the saline-treated *Mecp2*$^{-/+}$ mice. However, CPT157633-treated *Mecp2*$^{-/+}$ mice displayed a significant improvement in performance, although this was a partial restoration and did not achieve the WT levels of performance (Figure 5D). Furthermore, when CPT157633 treatment was stopped for 1 week and motor ability was re-tested, we observed that the improved motor ability that accompanied treatment was lost (Supplemental Figure 6A). This illustrates that the effects of CPT157633 are reversible and that prolonged treatment with the compound appears not to have adverse effects in these mice.

Finally, we examined maternal pup gathering, a natural social communication behavior. Proficiency in this behavior is achieved by experience-dependent learning in first-time mothers and virgin females cohoused with a mother and her pups (34–36). There are several advantages to assessing pup-gathering behavior in this context. First, we observed that deficiencies in this behavior are particularly robust in female *Mecp2*$^{-/+}$ mice. Second, the behavior relies critically on the detection of ultrasonic distress vocalizations by the female caregiver (37–39). Therefore, it requires interpretation of social information, an ability that is impaired in humans with RTT. Third, pup-gathering behavior has been functionally linked to the primary auditory cortex. Thus, pup-retrieval behavior is a robust and sensitive assay that assesses clinically relevant behavioral features and is mediated by a known neural circuit substrate. We tested the effect of PTP1B inhibition on the pup-retrieval behavior of both saline- and CPT157633-treated *Mecp2*$^{-/+}$ mice. Interestingly, when *Mecp2*$^{+/-}$ mice that had been treated with CPT157633 were subjected to the pup-retrieval paradigm, their latency — the time to gather pups back to the nest — improved (Supplemental Figure 6B). Collectively, the data illustrate that treatment with PTP1B inhibitors ameliorated the effects of disrupting MECP2 function in male and female mouse models of RTT.

Inhibition of PTP1B led to increased phosphorylation of TRKB, the receptor for BDNF. PTP1B has been validated as a major regulator of insulin and leptin signaling (19); however, as antidiabetic agents were insufficient to extend the lifespan of *Mecp2*$^{-/y}$-mutant male mice, we examined whether the beneficial effects of inhibition of PTP1B were associated with alteration of other pathways. We focused our attention on BDNF because of its role in sustaining several processes in the brain and the reports of efforts to improve BDNF signaling as an approach to addressing RTT (40–42).

First, we quantitated BDNF levels in the brain of WT and *Mecp2*-mutant mice. Although BDNF levels were decreased in both *Mecp2*$^{-/y}$ and *Mecp2*$^{-/+}$ mice compared with those in controls, BDNF was still present at 60% to 70% of the levels detected in the control WT mice (Figure 6, A and B). This was consistent with other reports (11, 43) and suggests that impaired BDNF signaling through its cognate receptor, rather than the loss of BDNF itself, may be a major contributing factor in these RTT models. Therefore, we examined the status of tyrosine phosphorylation and activation of the BDNF receptor tropomyosin-related kinase B (TRKB). We observed that tyrosine phosphorylation of TRKB was attenuated in saline-treated *Mecp2*$^{-/+}$ mice compared with that seen in the WT controls. In contrast, treatment with the PTP1B inhibitor CPT157633 resulted in enhanced tyrosine phosphorylation of TRKB in both WT and *Mecp2*$^{-/+}$ heterozygous female mice (Figure 6C).

In order to determine whether TRKB was a direct substrate of PTP1B, we investigated whether the PTP1B-D181A substrate–trapping mutant form of the phosphatase formed a stable complex with TRKB. Unlike the WT PTP1B enzyme, which dephosphorylates and releases the bound substrate, the substrate-trapping mutant PTP1B-D181A forms a stable complex with the bound substrate, which can be isolated and characterized (44). We generated brain lysates from PTP1B inhibitor–treated mice and incubated equal quantities of lysate with either WT or D181A substrate–trap-

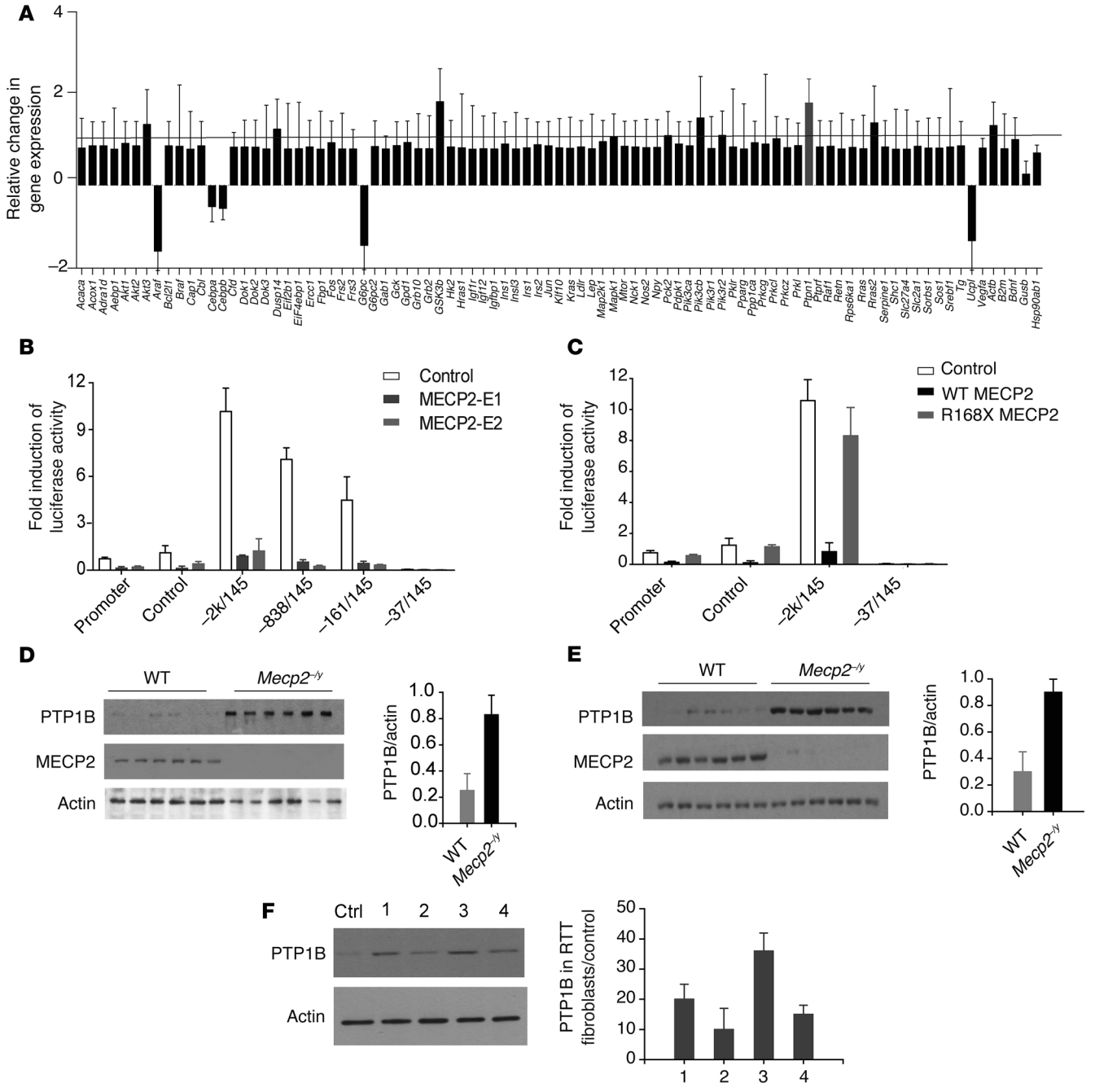

Figure 2. *Mecp2*-mutant mice expressed higher levels of PTP1B. (**A**) Total RNA obtained from WT and *Mecp2*$^{-/y}$ mice was reverse transcribed and the cDNA used in qPCR analysis. The relative change in gene expression in the insulin-signaling pathway in *Mecp2*$^{-/y}$ mice forebrain compared with WT was measured and the data normalized to *Gapdh* expression (n = 3, data represent the mean ± SEM). (**B**) A series of reporter constructs containing different lengths of the *PTPN1* promoter were expressed in HEK293T cells, together with control or MECP2-E1– or MECP2-E2–expressing plasmids. Expression of either isoform MECP2-E1 (light gray) or MECP2-E2 (dark gray) suppressed *PTPN1* promoter activity (n = 3, data represent the mean ± SEM). (**C**) Reporter constructs of the *PTPN1* promoter were expressed in HEK293T cells, together with control or WT MECP2– or R168X MECP2–expressing plasmids. Expression of of R168X MECP2 (gray), unlike WT MECP2 (black), failed to suppress *PTPN1* promoter activity (n = 3, data represent the mean ± SEM). (**D**) Immunoblots showing PTP1B levels in forebrain lysates obtained from *Mecp2*$^{-/y}$ and WT male mice; the same lysates were used to blot for MECP2 and the loading control actin. Graph shows quantitation of the immunoblots. All blots are representative of experiments performed 3 times. (**E**) Immunoblots showing PTP1B levels in forebrain lysates obtained from *Mecp2*$^{-/+}$ and WT female mice; the same lysates were used to blot for MECP2 and the loading control actin. Graph shows quantitation of the immunoblots. All blots are representative of experiments performed 3 times. (**F**) Immunoblots showing PTP1B levels in control and RTT patient–derived fibroblasts; the same lysates were used to blot for the loading control actin. Graph shows quantitation of the immunoblots. All blots are representative of experiments performed 3 times.

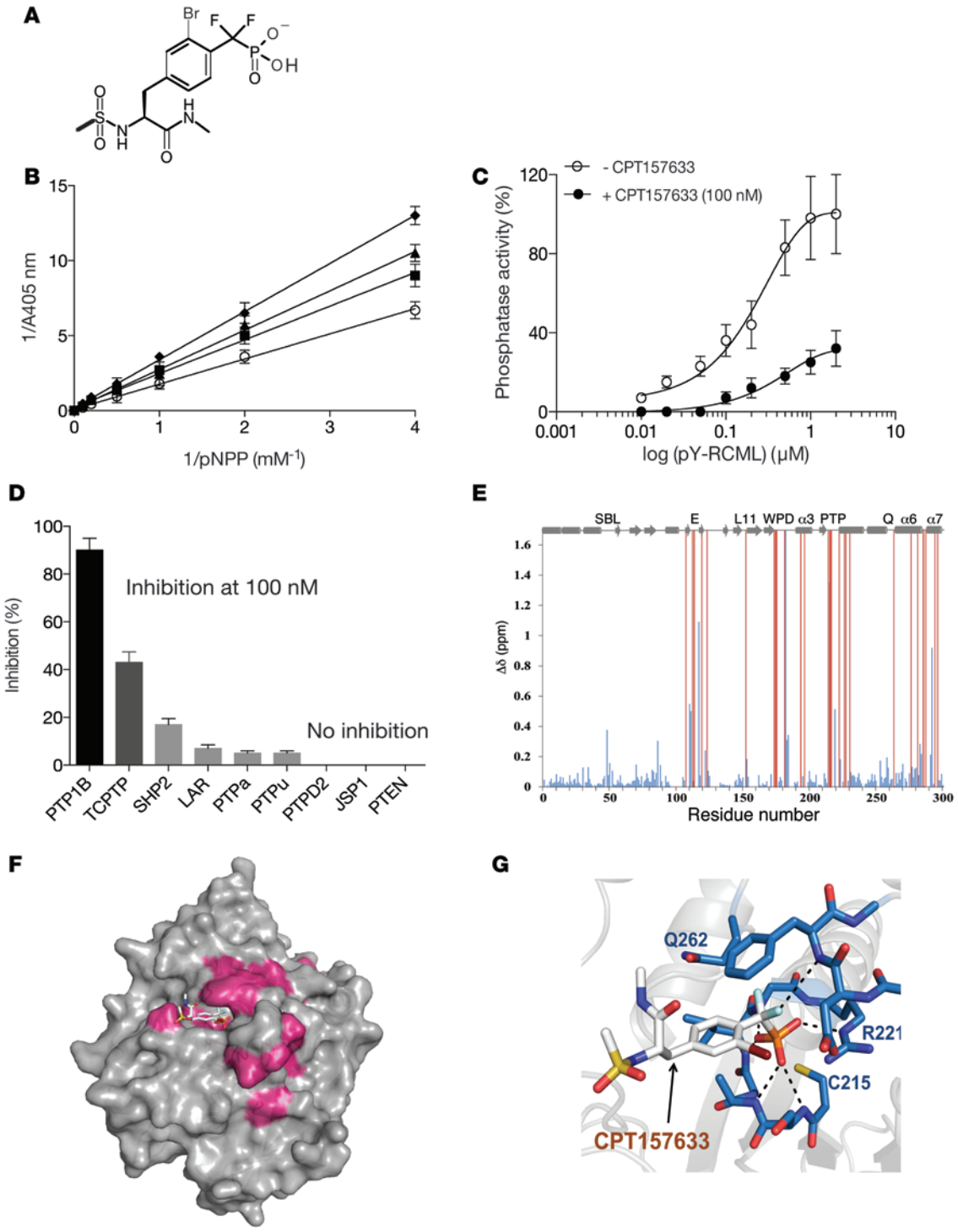

Figure 3. Biochemical characterization of the PTP1B inhibitor CPT157633. (**A**) Chemical structure of CPT157633. (**B**) Lineweaver-Burk plot for $PTP1B_{1-405}$ showing 1/rate versus 1/substrate at varying concentrations of CPT157633: 0 (white circles), 25 nM (black squares), 50 nM (black triangles), and 100 nM (black diamonds). The K_i was calculated to be 45 nM (n = 3, data are representative of 3 independent experiments). (**C**) PTP1B inhibition by CPT157633 was characterized using ^{32}P-RCML as a substrate. ^{32}P-RCML (0–1 μM) was titrated against PTP1B (10 nM) in the absence and presence of CPT157633 (100 nM) (n = 3, data are representative of 3 independent experiments). (**D**) Phosphatase activity of a panel of PTPs (10 nM) was tested in the absence and presence of CPT157633 (100 nM) using pNPP (2 mM) as a substrate (n = 3, data are representative of 3 independent experiments). (**E**) Titration of CPT157633 resulted mainly in CSPs localized to the residues that compose the PTP1B active site. Combined ^{1}H/^{15}N CSPs versus residues are shown, and the secondary structure of PTP1B is indicated. Blue indicates residues that are in fast exchange, and red indicates residues that broaden beyond detectability upon addition of CPT157633 or that were previously not assigned in the CPT157633 free form of PTP1B. (**F**) Overlay of PTP1B (gray surface) bound to CPT157633 inhibitor (orange). CSPs that accompanied binding of CPT157633 to PTP1B are mapped on to the structure (pink). (**G**) Electrostatic interactions between the CPT157633 inhibitor and the PTP1B active site loop (electrostatic interactions are indicated by black dashed lines).

ping mutant forms of PTP1B. We observed that TRKB formed a complex with the PTP1B-D181A substrate–trapping mutant, but not with the WT, active form of the phosphatase (Figure 6D). Furthermore, pretreatment of the PTP1B protein with pervanadate, which disrupts the active site of the enzyme, prevented binding to TRKB. These data are consistent with TRKB being a direct substrate of PTP1B.

Our previous structural studies highlighted the importance of an Asp/Glu–p-Tyr–p-Tyr–Arg/Lys sequence motif for optimal substrate recognition by PTP1B (28). The BDNF receptor TRKB contains such a motif in its activation loop (28); therefore, we examined the site specificity of the effects of PTP1B on this PTK using SH-SY5Y as a model system. In order to define which phosphorylation sites were targeted by PTP1B, we expressed WT and mutant (YY705/706FF, Y516F, and Y815F) forms of TRKB in SH-SY5Y cells. In response to BDNF stimulation, we noticed that the overexpressed TRKB was phosphorylated and activated only when the activation loop autophosphorylation sites were intact (Figure 6E). Lysates from cells expressing these various forms of TRKB were incubated with the PTP1B-D181A substrate–trapping mutant, which was then immunoprecipitated, and its interaction with TRKB was monitored. We found that PTP1B-D181A formed a stable complex with WT TRKB in response to BDNF stimulation. Mutation of both the activation loop residues Y705 and Y706 to phenylalanine (F) in TRKB abrogated this interaction (Figure 6F), whereas PTP1B-D181A was able to form a stable complex when residues Y516 and Y815 were mutated to phenylalanine (Figure 6F). Collectively, these data establish a direct enzyme-substrate interaction between PTP1B and phosphorylated Y705/706 (p-Y705/706) TRKB, the critical autophosphorylation sites that mediate BDNF-induced signaling.

Consistently, CPT157633 treatment resulted in enhanced tyrosine phosphorylation of Y705/Y706 TRKB in *Mecp2*$^{-/+}$ brain (Figure 6G). We also looked at the phosphorylation status of the 2 closely related TRK receptors TRKA and TRKC in response to CPT157633 treatment in brain lysates obtained from *Mecp2*$^{-/+}$ mice (Figure 6, H and I). Interestingly, the effects of PTP1B inhibition by CPT157633 on phosphorylation of TRKA or TRKC receptors were less pronounced than those on TRKB. Therefore, the data are consistent with a role of PTP1B as an inhibitor of BDNF/TRKB signaling that can be overcome by specific small-molecule inhibitors of the phosphatase and suggest a possible mechanism for the effects of the PTP that we observed in the RTT mouse models.

Discussion

In this study, we have demonstrated that MECP2 normally suppressed the expression of the protein tyrosine phosphatase PTP1B and that disruption of MECP2 resulted in elevated levels of this phosphatase in RTT models. Consequently, overexpression of PTP1B has the potential to be a specific marker of RTT, suggesting that PTP1B may be an ideal therapeutic target. We have shown that administration of small-molecule inhibitors of PTP1B dramatically extended the lifespan of *Mecp2*$^{-/y}$-null male mice and improved neural and behavioral symptoms of *Mecp2*$^{-/+}$ heterozygous female mice, illustrating that inhibition of the phosphatase led to amelioration of some of the phenotypes in these models of RTT. The data also identify PTP1B as a critical phosphatase for attenuating BDNF-induced signaling through the TRKB protein tyrosine kinase. This suggests that in RTT, functional loss of MECP2 causes an increase in PTP1B expression, which may then serve as a barrier to shift the signaling equilibrium more toward the inactive state of TRKB, resulting in impaired BDNF signaling (Figure 7). Therefore, this study, for the first time to our knowledge, presents PTP1B as a potential mechanism-based therapeutic target for RTT.

PTP1B is recognized as an antagonist of insulin and leptin signaling (19, 45). As *Mecp2*-mutant mice exhibited characteristics of both insulin and leptin resistance, we reasoned that upregulation of PTP1B may be of importance in contributing to disruption of the glucose homeostasis that accompanies *Mecp2* mutation in these RTT models. Whole-body knockout of PTP1B produced mice with enhanced insulin sensitivity and resistance to obesity induced by a high-fat diet (19, 45). Subsequent tissue-specific knockouts revealed that PTP1B in the brain plays a major role in the control of body mass and adiposity (45). As a regulator of signaling in response to leptin, a hormone that is produced by adipose tissue and exerts its physiological effect through signals in the hypothalamus that control appetite, PTP1B plays a key role in food intake and BW (45). In addition, leptin has been shown to facilitate the induction of long-term potentiation by increased transmission through the NMDA receptor (46), suggesting a potential role for leptin and PTP1B in learning and memory. Patients with RTT have been shown to display phenotypes that are consistent with abnormal function of the hypothalamus (16). Furthermore, deletion of MECP2 in *Sim1*-expressing neurons in the hypothalamus generated mice that displayed enhanced response to stress and abnormal social behavior. In addition, these animals were hyperleptinemic and displayed increased BW and body fat deposition associated with increased food intake (16). This phenotype suggests a classical leptin-resistant state, as would be encountered in the presence of elevated PTP1B, consistent with a role for the phosphatase in contributing to RTT pathogenesis. Interestingly, plasma levels of leptin have also been shown to be markedly elevated in patients with RTT (47, 48), which is one of the hallmarks of leptin resistance that is observed in metabolic disorders. However not all patients with elevated leptin levels were obese, which suggests that leptin accumulation in patients with RTT could be related to factors other than weight control and adiposity and that correcting circulating levels of leptin could have a beneficial effect on other aspects of RTT.

The IR is distributed widely in the brain and has been implicated in the control of synaptic function and dendritic architecture, which suggests a role in the development and function of neural circuits (49). Reduced insulin signaling in the brain has been shown to contribute to impaired learning and memory, resulting in cognitive deficits (49, 50). Interestingly, PTP1B is expressed in hippocampal neurons, where it has been shown to regulate learning behavior (51). Thus, antagonism of insulin signaling, as would accompany conditions that promote elevated PTP1B expression, may contribute to compromised learning ability. Nevertheless, the observation that the antidiabetic agents metformin, rosiglitazone, and AICAR restore glucose homeostasis in *Mecp2*-null male mice, but unlike PTP1B inhibitors do not

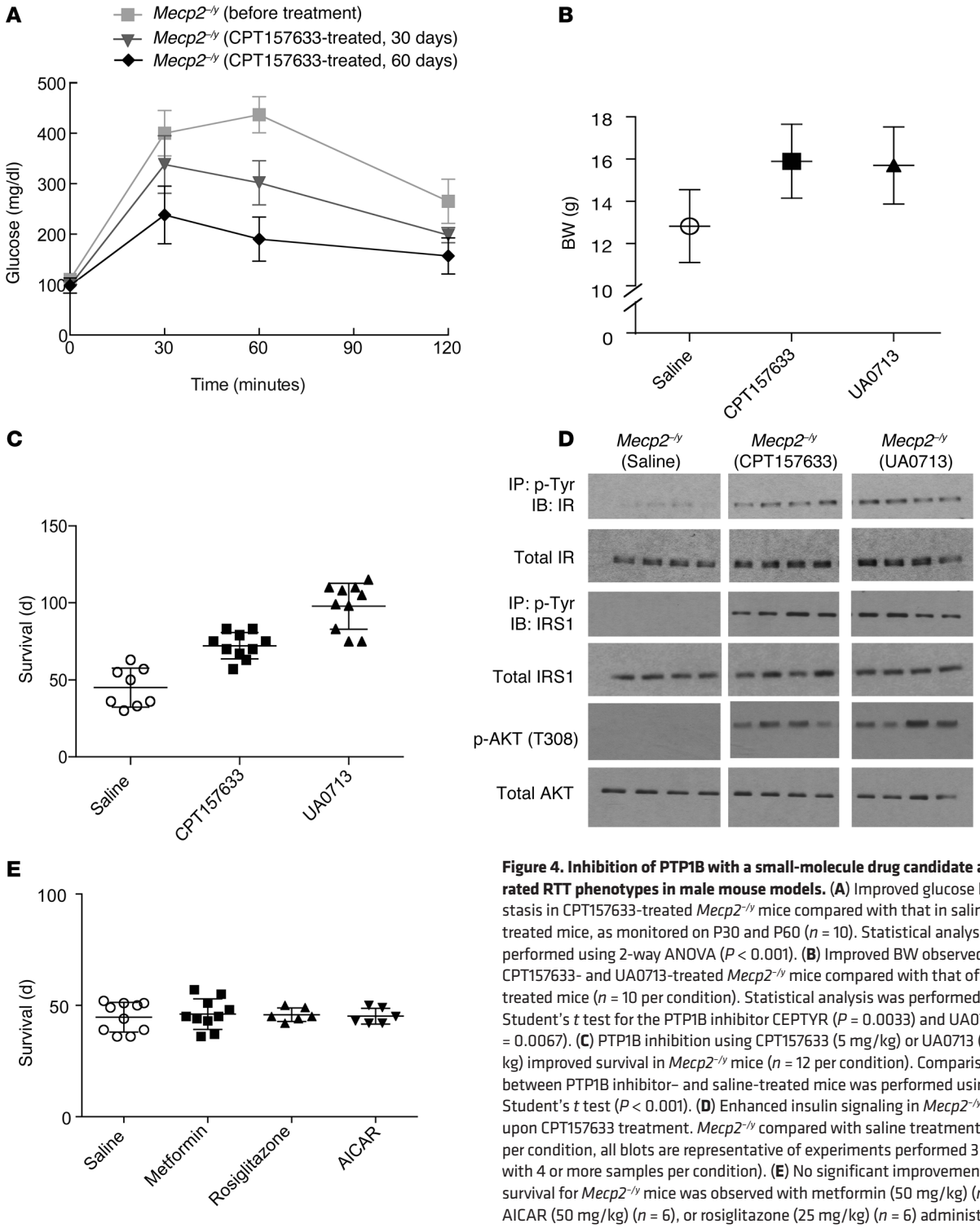

Figure 4. Inhibition of PTP1B with a small-molecule drug candidate ameliorated RTT phenotypes in male mouse models. (**A**) Improved glucose homeostasis in CPT157633-treated *Mecp2*$^{-/y}$ mice compared with that in saline-treated mice, as monitored on P30 and P60 (n = 10). Statistical analysis was performed using 2-way ANOVA ($P < 0.001$). (**B**) Improved BW observed with CPT157633- and UA0713-treated *Mecp2*$^{-/y}$ mice compared with that of saline-treated mice (n = 10 per condition). Statistical analysis was performed using Student's t test for the PTP1B inhibitor CEPTYR ($P = 0.0033$) and UA0713 ($P = 0.0067$). (**C**) PTP1B inhibition using CPT157633 (5 mg/kg) or UA0713 (5 mg/kg) improved survival in *Mecp2*$^{-/y}$ mice (n = 12 per condition). Comparison between PTP1B inhibitor– and saline-treated mice was performed using Student's t test ($P < 0.001$). (**D**) Enhanced insulin signaling in *Mecp2*$^{-/y}$ mice upon CPT157633 treatment. *Mecp2*$^{-/y}$ compared with saline treatment (n = 4 per condition, all blots are representative of experiments performed 3 times, with 4 or more samples per condition). (**E**) No significant improvement in survival for *Mecp2*$^{-/y}$ mice was observed with metformin (50 mg/kg) (n = 10), AICAR (50 mg/kg) (n = 6), or rosiglitazone (25 mg/kg) (n = 6) administration. Student's t test was used to evaluate the significance for metformin ($P = 0.02$), AICAR ($P = 0.03$), and rosiglitazone ($P = 0.08$).

extend lifespan, would suggest that the increase in PTP1B levels that we observed in *Mecp2*-mutant mice would be associated with suppression of other signaling pathways in addition to the response to insulin and leptin.

We demonstrated that PTP1B recognized TRKB as a direct substrate and that elevated PTP1B expression led to suppression of TRKB phosphorylation in *Mecp2*-mutant mice. Consistent with our observation, BDNF/TRKB signaling was recently shown to be augmented in the brains of PTP1B-knockout mice (52). This is of potential importance, because BDNF is also recognized as a target of MECP2 (42), thus implicating it in the etiology of RTT, and BDNF signaling is essential for various neuronal processes such as

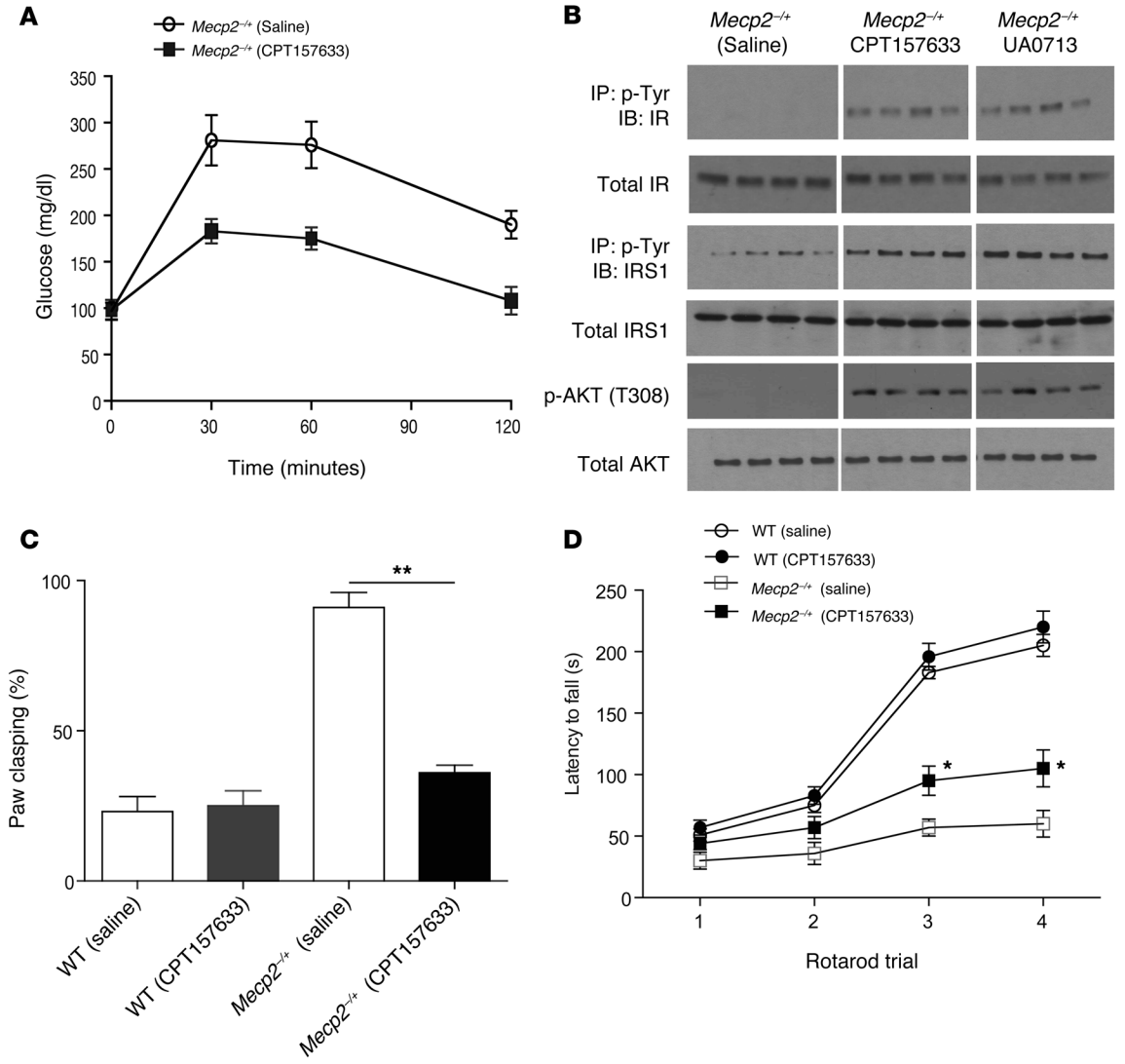

Figure 5. Inhibition of PTP1B with CPT157633 ameliorated RTT phenotypes in female mouse models. (**A**) GTT results for *Mecp2*$^{-/+}$ mice treated with saline or CPT157633 (5 mg/kg) (n = 10). (**B**) Representative immunoblots showing enhanced insulin signaling in *Mecp2*$^{-/+}$ mice upon CPT157633 treatment compared with mice receiving saline treatment. All blots are representative of experiments performed 3 times (n = 4). (**C**) For the paw-clasping assay, mice were suspended by their tails and observed for 30 seconds. The duration for which animals clasped their paws was used to calculate the percentage (n = 18 per condition). Data represent the SEM; statistical analysis was performed using a paired Student's t test (**P = 0.001). (**D**) Latency to fall from the rotarod for saline- and CPT157633-treated WT and *Mecp2*$^{-/+}$ mice (n = 10 per condition). Data represent the SEM; statistical analysis was performed using ANOVA (*P < 0.01).

cell survival, neurite growth, regulation of the inhibitory-excitatory balance, regulation of synapse formation, stabilization, and potentiation. BDNF signaling is initiated when the neurotrophic factor binds to the protein tyrosine kinase TRKB, the activation of which initiates important signaling responses (53). On the one hand, TRKB activation and tyrosine phosphorylation provide a docking site for the scaffolding protein SHC, which mediates activation of RAS/ERK and PI3K/AKT signaling pathways. On the other hand, TRKB activation recruits phospholipase-Cγ (PLCγ), which leads to mobilization of Ca^{2+} stores and activation of CaMKII and terminates in the activation of a transcriptional machinery initiated by the cAMP response element –binding (CREB) protein. Therefore, BDNF signaling through TRKB regulates transcription by mediating CREB translocation, protein translation through activation of the AKT/mTOR signaling pathway, and also mitogenic signaling through the RAS/MAPK signaling pathway (54). This would be consistent with an important role for PTP1B in multiple signaling contexts.

Although RTT is a monogenic disorder primarily caused by loss-of-function mutations in *MECP2*, there is a broad range of phenotypes associated with the myriad functions of MECP2. The search for phenotypic features in common in patients with RTT and in mouse models has illustrated the importance of metabolic changes, including disruption in mitochondrial function (55) and aberrant regulation of cholesterol metabolism (14). It is interesting to note that mice lacking PTP1B due to targeted disruption of the *Ptpn1* gene display a positive lipid profile with reduced circulating triglycerides and cholesterol, even under high-fat diet conditions. Hence, it is tempting to speculate that the metabolic effects of pharmacological inhibition of PTP1B may also help to ameliorate these general symptoms associated with RTT pathology.

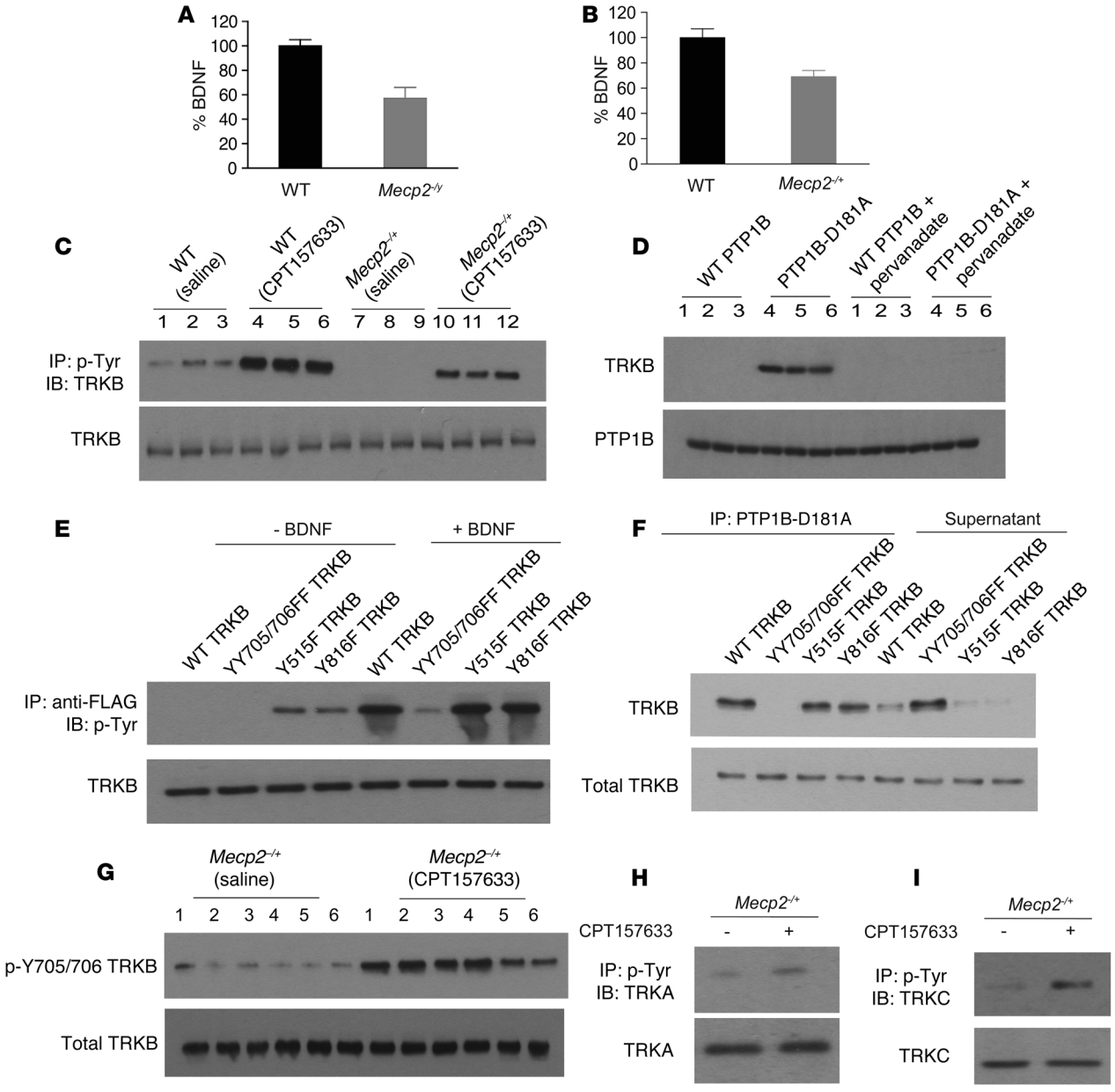

Figure 6. Inhibition of PTP1B led to increased phosphorylation of TRKB and enhanced signaling in response to BDNF. (**A**) BDNF levels measured by ELISA in the forebrains of P30 *Mecp2*$^{-/y}$ mice (gray bar) compared with WT animals (black bar) (n = 10, Student's t test, P = 0.015). (**B**) BDNF levels measured by ELISA in the forebrains of 10-week-old *Mecp2*$^{-/+}$ mice (gray bar) compared with WT animals (black bar) (n = 10, Student's t test, P = 0.023). (**C**) Tyrosine-phosphorylated proteins were immunoprecipitated from saline- and CPT157633-treated WT or *Mecp2*$^{-/+}$ mice, and immunoprecipitates were blotted for TRKB (upper panel). TRKB levels in each sample were measured by immunoblotting the lysate with anti-TRKB antibody (lower panel). (**D**) Brain lysates obtained from CPT157633-treated WT female mice were incubated with WT PTP1B or substrate-trapping mutant PTP1B-D181A, in the presence or absence of pervanadate. PTP1B immunoprecipitates were subjected to SDS-PAGE and immunoblotted with an antibody recognizing TRKB (upper panel) and PTP1B (lower panel). (**E**) WT and mutant forms of FLAG-TRKB were expressed in SH-SY5Y cells. Unstimulated and BDNF-stimulated cells were lysed and subjected to immunoprecipitation using anti-FLAG antibody. The immunoprecipitated samples were resolved on SDS gels and immunoblotted using the anti-phosphotyrosine antibody 4G10. (**F**) BDNF-stimulated lysates from SH-SY5Y cells expressing WT and mutant forms of TRKB were incubated with the substrate-trapping mutant form of PTP1B, and immunocomplexes were resolved on SDS gels and immunoblotted using anti-FLAG antibody to monitor the expression of TRKB. (**G**) Representative blot showing that CPT157633 treatment resulted in enhanced phosphorylation of Y705/Y706-TRKB on *Mecp2*$^{-/+}$ brain. (**H**) Representative blot showing the effects of CPT157633 treatment on tyrosine phosphorylation of the TRKA receptor in *Mecp2*$^{-/+}$ brain. (**I**) Representative blot showing the effects of CPT157633 treatment on tyrosine phosphorylation of the TRKC receptor in *Mecp2*$^{-/+}$ brain. All blots (**C**–**I**) are representative of experiments performed 3 times.

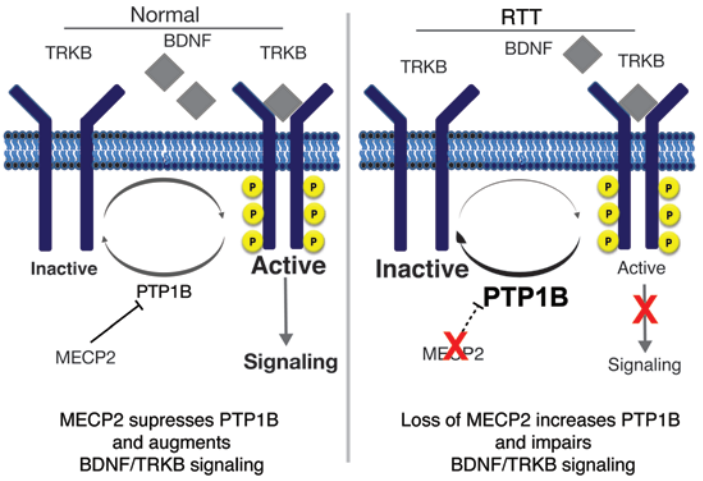

Figure 7. Model illustrating MECP2-mediated regulation of BDNF/TRKB signaling. MECP2 suppresses expression of PTP1B, which augments BDNF-induced signaling through the TRKB protein tyrosine kinase. Functional loss of MECP2 in RTT results in an increase in PTP1B levels, which attenuates BDNF/TRKB signaling.

Current therapeutic strategies for treating RTT have largely focused on BDNF and IGF-1 signaling pathways, from the perspective of trying to increase the levels of the growth factors and thereby restore a normal signaling response (11, 13). Our data suggest that an approach from a different but complimentary perspective may be more beneficial. Although decreased levels of BDNF have been reported in mouse models of RTT, our data indicate that there remain substantial amounts of the neurotrophin; in fact, the *Mecp2*-mutant mouse models examined in this study maintain BDNF at 60% to 70% of WT levels. This is further supported by 2 reports, which show that BDNF levels in cerebrospinal fluid or in the serum of patients with RTT are comparable to levels in unaffected individuals (56, 57). Therefore, our data suggest that BDNF resistance and suppression of the signaling response to BDNF, due to elevated levels of the inhibitory phosphatase PTP1B, may be an important contributing factor to the etiology of RTT. Consequently, current strategies aimed at supplying higher levels of the growth factor stimulus are unlikely to be effective due to their inability to overcome the barrier of elevated PTP1B. This is comparable to the situation in diabetes (insulin resistance) and obesity (leptin resistance), for which PTP1B is a validated therapeutic target. A better approach may be to alleviate the inhibitory constraint on the system by decreasing PTP1B activity with a small-molecule inhibitor, which would allow the cell to respond more effectively to available agonists.

Interestingly, when genetically defined autism candidate genes were ablated and transcriptomic analysis was conducted, it was observed that common signaling pathways were affected (58). This suggests that, despite the complex nature of autism spectrum disorders, with heterogeneity in behavioral and social impairments, there could be molecular mechanisms in common that may present an opportunity to target key regulatory checkpoints. Our new approach to therapeutic intervention in RTT using small-molecule drugs that target PTP1B and thereby targeting signaling pathways, including those that underlie metabolic regulation, also has implications for the treatment of other autism spectrum disorders and neurological diseases. For example, RAS/MAPK signaling has been identified as a regulator of activity-dependent protein synthesis, gene transcription, and mGluR-dependent synaptic plasticity, and disruption of the RAS/MAPK pathway has been associated with autism spectrum disorders (59, 60). Furthermore, metabolic disruption and obesity are becoming recognized as common features of autism spectrum disorders (18), suggesting that inhibition of PTP1B may also have a positive impact in those cases. Also, the utility of targeting PTP1B may not be restricted to autism spectrum disorders. For example, increased levels of PTP1B have been noted in a mouse model of Alzheimer's disease (61). Furthermore, mutations in MECP2 have been identified in other neurological diseases, such as schizophrenia (62), and it will be interesting to determine the extent to which this leads to alterations in PTP1B expression.

In conclusion, we have identified what we believe to be a novel therapeutic target and a novel strategy for the treatment of RTT. The identification of PTP1B as a therapeutic target highlights the possibility that some neurological disorders, such as RTT, may be viewed as reversible conditions that may be addressed through the manipulation of classical signaling pathways with small-molecule drugs. The prevalence of metabolic disruption and the importance of BDNF in other neuropsychiatric conditions, including autism spectrum disorders, further reinforces the potential to address a broad range of such conditions by this approach. With its extensive validation as a therapeutic target for treatment of diabetes and obesity, PTP1B has been the subject of drug development efforts for several years. Nevertheless, these efforts have been frustrated by technical challenges arising from the chemistry of PTP-mediated catalysis that have impeded the generation of inhibitors that target the active site but maintain appropriate pharmacokinetic and pharmacodynamic properties (19). However, this industry-imposed hurdle of oral bioavailability does not apply to all disease indications, including those for diseases such as RTT. Therefore, we hope that the results of this study will reinvigorate interest in PTP1B as a therapeutic target and open new opportunities to exploit this and other PTPs for the treatment of major human diseases.

Methods

Mice. B6.129-MeCP2$^{tm1.1Bird/J}$ mice, purchased from The Jackson Laboratory (stock number 003890), were used in this study. CBA/CaJ mice were used in the pup-retrieval assays.

Drug administration. CPT157633 (CEPTYR Inc.) and UA0713 (The Chemistry Research Solution [TCRS] LLC) were dissolved in sterile saline solution and administered i.p. or s.c. CPT157633 was given at a single dose of 5 mg/kg BW every day, and UA0713 was given at a dose of 5 mg/kg every other day. With WT and *Mecp2*$^{-/y}$ male mice, compound administration was initiated at P2, and for WT and *Mecp2*$^{-/+}$ female mice, compound administration was initiated at 10 weeks of age.

Antibodies and reagents. All reagents were purchased from Sigma-Aldrich unless otherwise specified. The antibodies used

in the study were directed against PTP1B (catalog 04-1140, clone EP1841Y; EMD Millipore); 4G10 (catalog 05-321, clone 4G10; Upstate Biotechnology); pY1162/1163-IR-β (catalog 700393, clone 97H9L7; Invitrogen); IR-β (catalog sc-711, clone C711; Santa Cruz Biotechnology Inc.); FLAG (catalog F3040, clone M1) and actin (catalog A2228, clone AC-74) (from Sigma-Aldrich); and IRS1 (catalog 2382, clone 59G8), p-T308 AKT (catalog 13038, clone D25E6), p-AKT (S473) (catalog 4051, clone 587F11), AKT (catalog 4691, clone C67E7), p-TFOXO1 (catalog 2599, clone 4G6), FOXO1 (catalog 2880, clone C29H4), p-GSK3β (catalog 8452, clone D1G2), GSK3β (catalog 12456, clone D5C5Z), p-Y705/706 TRKB (catalog 4621, clone C50F3), pY515 TRKB (catalog 4619, clone C53G9), TRKB (catalog 4603, clone 80E3, and MECP2 (catalog 3456, clone D4F3) (all from Cell Signaling Technology). Control and RTT patient–derived fibroblasts were obtained from the Corriell repository. TRKA and TRKC expression constructs were a gift of Moses Chao (NYU Medical Center, New York, New York, USA).

Identification of TRKB as a substrate of PTP1B. Substrate identification experiments were performed as described previously (44). Brain lysates (1 mg/ml) obtained from saline- and/or PTP1B inhibitor–treated WT and *Mecp2*$^{-/+}$ female mice were incubated with 20 μl His-tagged WT PTP1B and PTP1B-D181A fusion protein coupled to beads (10 μg/μl) in the presence and absence of 1 mM pervanadate. After several washes, complexes were analyzed by immunoblotting. SH-SY5Y cells were cultured in DMEM supplemented with 10% FCS, 200 mM L-glutamine, nonessential amino acids (NEAA) (×100, HyClone; GE Healthcare Life Sciences), and gentamycin (10 mg/ml; Invitrogen) at 37°C and 5% CO_2 in a humidified atmosphere. Cells were differentiated by treatment with 10 μM retinoic acid for 7 days. These cells were used for all TRKB phosphorylation–related experiments by stimulating cells with varying concentrations of BDNF (0–100 ng/ml). PTP1B inhibitor (0–10 μM) treatment was performed for 1 hour prior to stimulation. For transfection of SH-SY5Y cells, pFLAG-TRKB, pFLAG-Y515F TRKB, pFLAG-Y705F/Y706F TRKB, pFLAG-Y816F TRKB, and pCDNA-PTP1B were used. The TRKB constructs were a gift of James McNamara (Duke University, Durham, North Carolina, USA). Cells were seeded in 6-well plates at a density of 5×10^5 cells per well. After 24 hours, cells were transfected for 24 hours with FuGENE HD Transfection Reagent (Roche) according to the manufacturer's protocol. Next, the cells were used for stimulation with BDNF, without or with PTP1B inhibitor treatment.

PTPN1 promoter assay. HEK293T cells were transfected using Lipofectamine Reagent (Life Technologies) according to the manufacturer's protocol. Typically, 1 μg of the reporter plasmid containing different lengths of the promoter was used along with 1 μg pRL-TK (Promega), an expression vector containing cDNA encoding *Renilla* luciferase, as an internal control for transfection efficiency. Approximately, 1.0×10^5 cells were used for each transfection with Lipofectamine Reagent (Life Technologies) in a 24-well plate. One microgram of the reporter plasmid for expression of firefly luciferase was used. Expression plasmids for either human MECP2-E1 (0.1 μg/ml), MECP2-E2 (0.1 μg/ml), or control plasmid without an insert (0.1 μg/ml) were cotransfected. Cells were incubated with a DNA-lipid complex for 24 hours and washed with PBS, and luciferase activity was assayed using the Dual-Luciferase Reporter Assay System (Promega).

Paw-clasping assay. For the paw-clasping assay, mice were suspended by their tails and observed for 30 seconds. The duration for which animals clasped their paws was used to calculate the percentage (paw clasping [%] = [time spent clasping paws (s)/30(s)] × 100). Age-matched mice (*Mecp2*$^{-/+}$ vehicle-treated mice, $n = 18$; CPT157633-treated mice, $n = 18$) were used.

Rotarod performance. An increasing angular-speed rotarod system (AccuScan Instruments) was used on 12- to 14-week-old female mice. Both WT and *Mecp2*$^{-/+}$ mice were acclimated to the testing apparatus with three 90-second trials of steadily increasing speed (4–6 rpm). Following this acclimation, 4 trials were conducted. These trials were repeated the following day without an acclimation period. The latency to fall for each trial was recorded.

Protein expression and purification for NMR studies. The PTPT1B catalytic domain (residues 1–301; $PTP1B_{1–301}$) was expressed in *E. coli* and purified as previously described (63). Briefly, isotope-labeled $PTP1B_{1–301}$ was expressed in *E. coli* cultures grown in M9 minimal media containing 1 g/l ^{15}N NH_4Cl, 100% D_2O, and either 4 g/l ^{13}C-D-glucose or ^{12}C-D-glucose. Cultures were grown at 37°C to an OD_{600} of approximately 0.6 under vigorous shaking (250 rpm). Protein expression was induced with the addition of 1 mM isopropyl β-D-thiogalactopyranoside (IPTG), and cultures were incubated for approximately 20 hours at 18°C and shaken at 250 rpm. Protein yields were approximately 46 mg/l in Luria broth, approximately 34 mg/l in ^2H,^{15}N M9 medium, and approximately 17 mg/l in ^2H,^{15}N,^{13}C M9 medium. $PTP1B_{1–301}$ was purified by Ni^{2+}-affinity chromatography and size exclusion chromatography (SEC) (Superdex 75 26/60), with 50 mM HEPES, pH 6.8, 150 mM NaCl, 0.5 mM Tris [2-carboxyethyl] phosphine (TCEP) as the final NMR buffer.

NMR spectroscopy. NMR data were collected on a Bruker AVANCE III HD 850 MHz spectrometer equipped with a TCI HCN *Z*-gradient cryoprobe at 298 K. NMR measurements of $PTP1B_{1–301}$ were recorded using either ^2H,^{15}N- or ^2H,^{15}N,^{13}C-labeled protein at a final concentration of 0.2 mM in 50 mM HEPES, pH 6.8, 150 mM NaCl, 0.5 mM TCEP, and 90% H_2O/10% D_2O. The sequence-specific backbone assignment of $PTP1B_{1–301}$ in the CPT157633-bound state was achieved using the following experiments at 850 MHz ^1H Larmor frequency: 2D [^1H,^{15}N] TROSY, 3D TROSY-HNCA, and 3D TROSY-HN(CO)CA. Assignment and titration spectra were processed with Topspin 3.1 (Bruker), and data were evaluated using Sparky software (http://www.cgl.ucsf.edu/home/sparky/).

NMR analysis of inhibitor binding. CPT157633 was titrated into 200 μM [^2H,^{15}N]-PTP1B at molar ratios of 0.1:1, 0.2:1, 0.4:1, 0.5:1, 1:1, 1.5:1, 3:1, and 5:1. CPT157633:$PTP1B_{1–301}$ and 2D [^1H,^{15}N] TROSY spectra were recorded for each titration point. CPT157633 was solubilized in water at 100 mM. Chemical shift differences (Dd) between $PTP1B_{1–301}$ and CPT157633-bound $PTP1B_{1–301}$ (1.5:1 molar ratio) spectra were calculated using the following equation:

$$\Delta\delta(ppm) = \sqrt{(\Delta\delta_H)^2 + \left(\frac{\Delta\delta_N}{10}\right)^2}$$

(Equation 1)

All chemical shifts for CPT157633-bound PTP1B were deposited in the BioMagResBank (http://www.bmrb.wisc.edu) under accession number 25375.

Crystallization and structure determination. $PTP1B_{1–301}$ was purified as previously described (63), with the exception that the final protein buffer was 20 mM Tris, pH 7.5, 25 mM NaCl, 0.2 mM EDTA, and 0.5 mM TCEP. CPT157633 (10:1 molar ratio) was added to PTP1B to form $PTP1B_{1–301}$:CPT157633, and the protein:ligand complex was concentrated to 50 mg/ml for crystallization. Crystals of $PTP1B_{1–301}$:CPT157633 were obtained using sitting-drop vapor diffusion in 0.1 M Tris, pH 7.4, 20% PEG 8000, and 0.2 M $MgCl_2$. The small initial crystals were used as seeds for subsequent crystallization trials in the same mother liquor. Crystals were cryoprotected by a 10-second soak in mother liquor, supplemented with 30% glycerol and 10% CPT157633 (100 μM) and immediately flash-frozen in liquid nitrogen. X-ray data were collected on a single crystal at 112 K using a Rigaku FR-E+ SuperBright rotating copper anode x-ray generator with a Saturn 944 HG CCD detector (Brown University Structural Biology Facility), and the data were processed to 1.9 Å. The $PTP1B_{1–301}$:CPT157633 data were phased using molecular replacement (Phaser, as implemented in PHENIX; ref. 64), with PTP1B (PDBID:1C88; ref. 65) as the search model. Clear electron density for the bound CPT157633 was visible in the initial maps. The initial model of $PTP1B_{1–301}$:CPT157633 was built using Phenix.AutoBuild (64), followed by iterative rounds of refinement in PHENIX and manual building using Coot (66). The Restraint file for the CPT157633 ligand was generated with Phenix.eLBOW (64) using the CPT157633 smiles string CNC(=O)[C@H](Cc1ccc(C(F)(F)P(=O)(O)O)c(Br)c1)NS(C)(=O)=O. Data collection and refinement statistics are reported in Supplemental Table 2. All coordinates for CPT157633-bound PTP1B were deposited in the Protein Data Bank (PDB) under accession number 4Y14.

Statistics. All results are expressed as the mean ± SEM. ANOVA and a 2-tailed Student's *t* test were used to determine statistical significance. A *P* value of 0.05 or less was considered significant. Statistical analysis and generation of graphs were performed using GraphPad Prism, version 7 (GraphPad Software).

Study approval. All study protocols involving mice were approved by the IACUC of the CSHL and conducted in accordance with NIH guidelines for the care and use of animals.

Acknowledgments

We thank Nick Pombonyo (summer student, Sacred Heart University, Fairfield, Connecticut, USA) for his help with the ChIP-PCR analysis. This research was supported by NIH grants CA53840 and GM55989 (to N.K. Tonks); NIH grant MH082808 (to L. Van Aelst); a CSHL Cancer Centre Support grant (CA45508); and by an American Diabetes Association Pathway to Stop Diabetes grant (1-14-ACN-31, to W. Peti). This research is based in part on data obtained at the Brown University Structural Biology Core Facility, which is supported by the Division of Biology and Medicine of Brown University.

Address correspondence to: Nicholas K. Tonks, Cold Spring Harbor Laboratory, 1 Bungtown Rd., Cold Spring Harbor, New York 11724, USA. Phone: 516.367.8846; E-mail: tonks@cshl.edu.

1. Chapleau CA, Lane J, Pozzo-Miller L, Percy AK. Evaluation of current pharmacological treatment options in the management of Rett syndrome: from the present to future therapeutic alternatives. *Curr Clin Pharmacol*. 2013;8(4):358–369.
2. Percy AK, et al. Rett syndrome diagnostic criteria: lessons from the Natural History Study. *Ann Neurol*. 2010;68(6):951–955.
3. Villard L. MECP2 mutations in males. *J Med Genet*. 2007;44(7):417–423.
4. Amir RE, Van den Veyver IB, Wan M, Tran CQ, Francke U, Zoghbi HY. Rett syndrome is caused by mutations in X-linked MECP2, encoding methyl-CpG-binding protein 2. *Nat Genet*. 1999;23(2):185–188.
5. Shahbazian MD, Zoghbi HY. Molecular genetics of Rett syndrome and clinical spectrum of MECP2 mutations. *Curr Opin Neurol*. 2001;14(2):171–176.
6. Ausio J, de Paz AM, Esteller M. MeCP2: the long trip from a chromatin protein to neurological disorders. *Trends Mol Med*. 2014;20(9):487–498.
7. Guy J, Hendrich B, Holmes M, Martin JE, Bird A. A mouse Mecp2-null mutation causes neurological symptoms that mimic Rett syndrome. *Nat Genet*. 2001;27(3):322-6.
8. Shepherd GM, Katz DM. Synaptic microcircuit dysfunction in genetic models of neurodevelopmental disorders: focus on Mecp2 and Met. *Curr Opin Neurobiol*. 2011;21(6):827–833.
9. Kavalali ET, Nelson ED, Monteggia LM. Role of MeCP2, DNA methylation, and HDACs in regulating synapse function. *J Neurodev Disord*. 2011;3(3):250–256.
10. Percy AK. Neuroscience. Path to treat Rett syndrome. *Science*. 2013;342(6156):318–320.
11. Deogracias R, et al. Fingolimod, a sphingosine-1 phosphate receptor modulator, increases BDNF levels and improves symptoms of a mouse model of Rett syndrome. *Proc Natl Acad Sci U S A*. 2012;109(35):14230–14235.
12. Kron M, Lang M, Adams IT, Sceniak M, Longo F, Katz DM. A BDNF loop-domain mimetic acutely reverses spontaneous apneas and respiratory abnormalities during behavioral arousal in a mouse model of Rett syndrome. *Dis Model Mech*. 2014;7(9):1047–1055.
13. Tropea D, et al. Partial reversal of Rett Syndrome-like symptoms in MeCP2 mutant mice. *Proc Natl Acad Sci U S A*. 2009;106(6):2029–2034.
14. Buchovecky CM, et al. A suppressor screen in Mecp2 mutant mice implicates cholesterol metabolism in Rett syndrome. *Nat Genet*. 2013;45(9):1013–1020.
15. Li Y, et al. Global transcriptional and translational repression in human-embryonic-stem-cell-derived Rett syndrome neurons. *Cell Stem Cell*. 2013;13(4):446–458.
16. Fyffe SL, et al. Deletion of Mecp2 in Sim1-expressing neurons reveals a critical role for MeCP2 in feeding behavior, aggression, and the response to stress. *Neuron*. 2008;59(6):947–958.
17. Cooke DW, Naidu S, Plotnick L, Berkovitz GD. Abnormalities of thyroid function and glucose control in subjects with Rett syndrome. *Horm Res*. 1995;43(6):273–278.
18. Herbert MR, Buckley JA. Autism and dietary therapy: case report and review of the literature. *J Child Neurol*. 2013;28(8):975–982.
19. Tonks NK. Protein tyrosine phosphatases — from housekeeping enzymes to master regulators of signal transduction. *FEBS J*. 2013;280(2):346–378.
20. Ricciardi S, et al. Reduced AKT/mTOR signaling and protein synthesis dysregulation in a Rett syndrome animal model. *Hum Mol Genet*. 2011;20(6):1182–1196.
21. Pitcher MR, et al. Insulinotropic treatments exacerbate metabolic syndrome in mice lacking MeCP2 function. *Hum Mol Genet*. 2013;22(13):2626–2633.
22. Bryant NJ, Govers R, James DE. Regulated transport of the glucose transporter GLUT4. *Nat Rev Mol Cell Biol*. 2002;3(4):267–277.
23. Fukada T, Tonks NK. Identification of YB-1 as a regulator of PTP1B expression: implications for regulation of insulin and cytokine signaling. *EMBO J*. 2003;22(3):479–493.
24. Fukada T, Tonks NK. The reciprocal role of Egr-1 and Sp family proteins in regulation of the PTP1B promoter in response to the p210 Bcr-Abl oncoprotein-tyrosine kinase. *J Biol Chem*. 2001;276(27):25512–25519.
25. Lindtner C, et al. Binge drinking induces whole-body insulin resistance by impairing hypothalamic insulin action. *Sci Transl Med*. 2013;5(170):170ra14.
26. Li D, Li W, Higai K, Koike K. Protein tyrosine phosphatase 1B inhibitory activities of ursane- and lupane-type triterpenes from Sorbus pohuashanensis. *J Nat Med*. 2014;68(2):427–431.
27. Zhang W, et al. Ursolic acid and its derivative inhibit protein tyrosine phosphatase 1B, enhancing insulin receptor phosphorylation and stimulating glucose uptake. *Biochim Biophys Acta*.

2006;1760(10):1505–1512.
28. Salmeen A, Andersen JN, Myers MP, Tonks NK, Barford D. Molecular basis for the dephosphorylation of the activation segment of the insulin receptor by protein tyrosine phosphatase 1B. *Mol Cell*. 2000;6(6):1401–1412.
29. Goldstein BJ, Bittner-Kowalczyk A, White MF, Harbeck M. Tyrosine dephosphorylation and deactivation of insulin receptor substrate-1 by protein-tyrosine phosphatase 1B. Possible facilitation by the formation of a ternary complex with the Grb2 adaptor protein. *J Biol Chem*. 2000;275(6):4283–4289.
30. Fryer LG, Parbu-Patel A, Carling D. The Anti-diabetic drugs rosiglitazone and metformin stimulate AMP-activated protein kinase through distinct signaling pathways. *J Biol Chem*. 2002;277(28):25226–25232.
31. Towler MC, Hardie DG. AMP-activated protein kinase in metabolic control and insulin signaling. *Circ Res*. 2007;100(3):328–341.
32. Katz DM, et al. Preclinical research in Rett syndrome: setting the foundation for translational success. *Dis Model Mech*. 2012;5(6):733–745.
33. Chahrour M, Zoghbi HY. The story of Rett syndrome: from clinic to neurobiology. *Neuron*. 2007;56(3):422–437.
34. Ehret G, Haack B. Categorical perception of mouse pup ultrasound by lactating females. *Die Naturwissenschaften*. 1981;68(4):208–209.
35. Ehret G, Koch M, Haack B, Markl H. Sex and parental experience determine the onset of an instinctive behavior in mice. *Die Naturwissenschaften*. 1987;74(1):47.
36. Cohen L, Rothschild G, Mizrahi A. Multisensory integration of natural odors and sounds in the auditory cortex. *Neuron*. 2011;72(2):357–369.
37. Lin HH, Chu LA, Fu TF, Dickson BJ, Chiang AS. Parallel neural pathways mediate CO2 avoidance responses in Drosophila. *Science*. 2013;340(6138):1338–1341.
38. Sewell GD. Ultrasonic communication in rodents. *Nature*. 1970;227(5256):410.
39. Smith JC. Responses of adult mice to models of infant calls. *J Comp Physiol Psych*. 1976;90(12):1105–1115.
40. Lu B, Nagappan G, Guan X, Nathan PJ, Wren P. BDNF-based synaptic repair as a disease-modifying strategy for neurodegenerative diseases. *Nat Rev Neurosci*. 2013;14(6):401–416.
41. Lu B, Nagappan G, Lu Y. BDNF and synaptic plasticity, cognitive function, and dysfunction. *Handb Exp Pharmacol*. 2014;220:223–250.
42. Katz DM. Brain-derived neurotrophic factor and Rett syndrome. *Handb Exp Pharmacol*. 2014;220:481–495.
43. Mellios N, et al. β2-Adrenergic receptor agonist ameliorates phenotypes and corrects microRNA-mediated IGF1 deficits in a mouse model of Rett syndrome. *Proc Natl Acad Sci U S A*. 2014;111(27):9947–9952.
44. Flint AJ, Tiganis T, Barford D, Tonks NK. Development of "substrate-trapping" mutants to identify physiological substrates of protein tyrosine phosphatases. *Proc Natl Acad Sci U S A*. 1997;94(5):1680–1685.
45. Tsou RC, Bence KK. Central regulation of metabolism by protein tyrosine phosphatases. *Front Neurosci*. 2012;6:192.
46. Harvey J. Leptin: a diverse regulator of neuronal function. *J Neurochem*. 2007;100(2):307–313.
47. Blardi P, et al. Long-term plasma levels of leptin and adiponectin in Rett syndrome. *Clin Endocrinol (Oxf)*. 2009;70(5):706–709.
48. Blardi P, et al. Rett syndrome and plasma leptin levels. *J Pediatr*. 2007;150(1):37–39.
49. Chiu SL, Cline HT. Insulin receptor signaling in the development of neuronal structure and function. *Neural Dev*. 2010;5:7.
50. Banks WA, Owen JB, Erickson MA. Insulin in the brain: there and back again. *Pharmacol Ther*. 2012;136(1):82–93.
51. Fuentes F, et al. Protein tyrosine phosphatase PTP1B is involved in hippocampal synapse formation and learning. *PLoS One*. 2012;7(7):e41536.
52. Ozek C, Kanoski SE, Zhang ZY, Grill HJ, Bence KK. Protein-tyrosine phosphatase 1B (PTP1B) is a novel regulator of central brain-derived neurotrophic factor and tropomyosin receptor kinase B (TrkB) signaling. *J Biol Chem*. 2014;289(46):31682–31692.
53. Skaper SD. The neurotrophin family of neurotrophic factors: an overview. *Methods Mol Biol*. 2012;846:1–12.
54. Minichiello L. TrkB signalling pathways in LTP and learning. *Nat Rev Neurosci*. 2009;10(12):850–860.
55. Muller M, Can K. Aberrant redox homoeostasis and mitochondrial dysfunction in Rett syndrome. *Biochem Soc Trans*. 2014;42(4):959–964.
56. Riikonen R. Neurotrophic factors in the pathogenesis of Rett syndrome. *J Child Neurol*. 2003;18(10):693–697.
57. Vanhala R, Korhonen L, Mikelsaar M, Lindholm D, Riikonen R. Neurotrophic factors in cerebrospinal fluid and serum of patients with Rett syndrome. *J Child Neurol*. 1998;13(9):429–433.
58. Pinto D, et al. Convergence of genes and cellular pathways dysregulated in autism spectrum disorders. *Am J Hum Genet*. 2014;94(5):677–694.
59. Zoghbi HY, Bear MF. Synaptic dysfunction in neurodevelopmental disorders associated with autism and intellectual disabilities. *Cold Spring Harb Perspect Biol*. 2012;4(3):a009886.
60. Ebert DH, Greenberg ME. Activity-dependent neuronal signalling and autism spectrum disorder. *Nature*. 2013;493(7432):327–337.
61. Mody N, Agouni A, McIlroy GD, Platt B, Delibegovic M. Susceptibility to diet-induced obesity and glucose intolerance in the APP (SWE)/PSEN1 (A246E) mouse model of Alzheimer's disease is associated with increased brain levels of protein tyrosine phosphatase 1B (PTP1B) and retinol-binding protein 4 (RBP4), and basal phosphorylation of S6 ribosomal protein. *Diabetologia*. 2011;54(8):2143–2151.
62. McCarthy SE, et al. De novo mutations in schizophrenia implicate chromatin remodeling and support a genetic overlap with autism and intellectual disability. *Mol Psychiatry*. 2014;19(6):652–658.
63. Krishnan N, et al. Targeting the disordered C terminus of PTP1B with an allosteric inhibitor. *Nat Chem Biol*. 2014;10(7):558–566.
64. Adams PD, et al. PHENIX: a comprehensive Python-based system for macromolecular structure solution. *Acta Crystallogr D Biol Crystallogr*. 2010;66(pt 2):213–221.
65. Iversen LF, et al. Structure-based design of a low molecular weight, nonphosphorus, nonpeptide, and highly selective inhibitor of protein-tyrosine phosphatase 1B. *J Biol Chem*. 2000;275(14):10300–10307.
66. Emsley P, Cowtan K. Coot: model-building tools for molecular graphics. *Acta Crystallogr D Biol Crystallogr*. 2004;60(pt 12 pt 1):2126–2132.